RESEARCH PAPER

Temperature Dependent Dynamic Response of Open-Cell Polyurethane Foams

D. Morrison[1] · J. Morton[1] · M. Foster[1,2] · L. Lamberson[1]

Abstract

Background Polyurethane foams have many uses ranging from comfort fitting seats and shoes to protective inserts in helmets and sports equipment. Current military helmet designs employ foam pads of varying densities and bulk material properties to help absorb energy from impacts ranging from quasi-static to ballistic level strain-rates.

Objective This study aims to analyze the thermomechanical uniaxial compression behavior of a high density liner foam pad and a low density liner foam pad used in the Advanced Combat Helmet. These experiments were conducted under strain-rates of 10^2 s^{-1} and under temperature conditions ranging from -20 to 40 °C. This temperature range was chosen to simulate desert and arctic conditions, with a strain-rate regime chosen to represent loads that would occur often throughout the life of the helmet, such as drops, bumps from riding in a vehicle, or heavy collisions from falling.

Method Multiple experimental apparatuses were used in this study, including a Shimadzu TCE-N300 thermostatic chamber (used to create the varying temperature environments) and a custom-built drop-test system (used to induce intermediate strain-rates). Every experiment was paired with two accelerometers and a high speed camera used for Digital Image Correlation (DIC) to analyze sample deformation and resultant acceleration. The foam's mechanical response and energy absorption properties were investigated from the measured stress-strain curves. Additionally, each foam composition was analyzed with X-ray computed micro-tomography (XCT) to investigate microstructure properties pre and post-mortem.

Results Results show that temperature decreased the energy absorption of the low density composition by 48% ± 5% as temperature changed from -20 °C to 40 °C, while energy absorption increased by 53% ± 16% for the high density composition over the same temperature.

Conclusion A comparison between the loading response and the material's density characteristics revealed that the foam's mechanical properties are heavily dependent on strain-rate applications, as well as environmental factors including temperature. Several important characteristics surrounding each foam composition's deformation mechanics and damage tolerance as a result of temperature are discussed.

Introduction

The use of cellular materials as protective insulation has continued to grow due to their unique energy absorption properties and loading responses [1–5]. Specifically, under

L. Lamberson is a member of SEM.

✉ L. Lamberson
  les@mines.edu

[1] Colorado School of Mines, Golden, CO 80401 , USA

[2] Lawrence Livermore National Laboratory, Livermore, USA

compressive loading, cellular materials maintain the ability to convert kinetic energy into strain energy through complex deformation mechanisms. The compressive response involves three distinct regions on a stress-strain curve. At the first instance of loading, cellular materials display a linear elastic zone, which peaks at a critical stress value. This is followed by a plateau, where an almost constant stress produces an increase in axial strain. The last region is a densification regime, where a large increase in stress results in a tapered increase in strain [1, 3, 4, 6–8], as shown in Fig. 1. The shape, length, and slope of these zones is dependent on the cellular solids microstructure and chemistry, which consists of a base
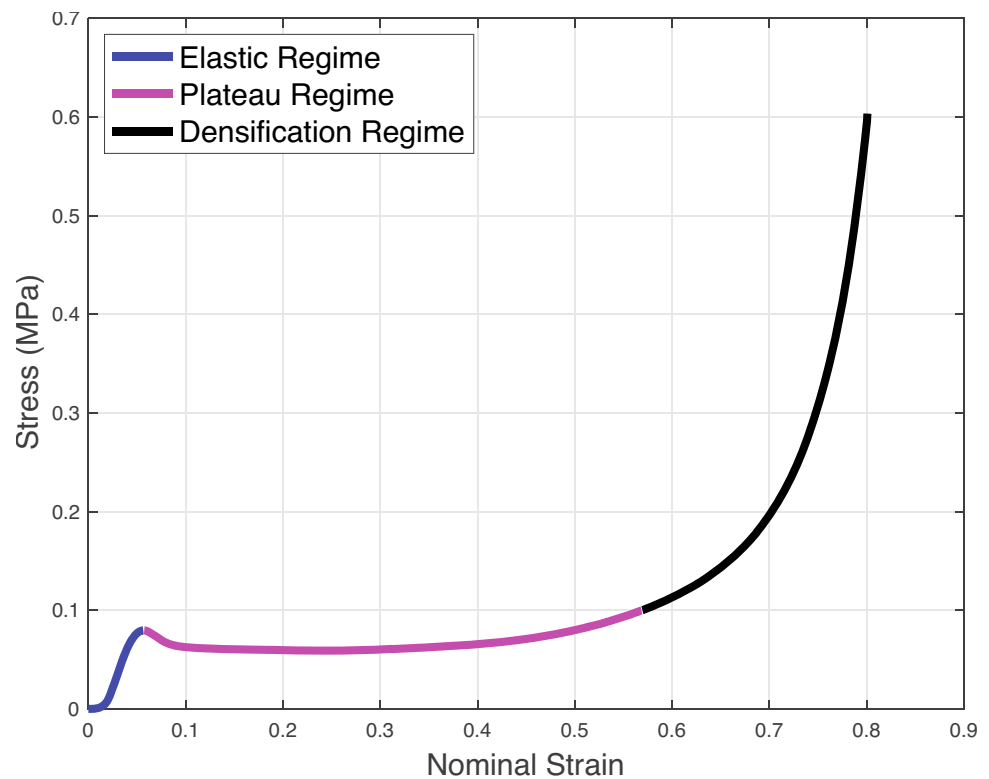
Fig. 1 General open-cell vis-
coelastic material stress-strain
curve highlighting the three
distinct deformation regimes

solid and a fluid that fills the space not occupied by the base material [9–11]. For most cellular solids, the base material is a polymer chain, such as polyurethane or polyurea. These polymer chains are viscoelastic, and are partially responsible for the material's rate-dependent response to loading conditions [2, 6, 12]. Since the development and fabrication of cellular solids can be fallible and thus challenging to model, the loading response of the polymer based material is largely characterized through experimentation. While a significant experimental effort has analyzed aspects of this response, the role of temperature in these results has not been as well studied. The effect of temperature is crucial for the modeling efforts around cellular solids, since cellular solids may be implemented and used in various environments [8, 13, 14]. Therefore, it is vital to analyze and experiment on cellular solids across a range of temperatures–from freezing to hot conditions [7, 10]. Understanding the role temperature plays in changing the energy absorption properties of a new polymer-based protective material allows for a better grasp of how an individual composition can be tailored for a specific environmental concern. Currently, it is not well known how the rate-dependent loading response and open-cell polymer microstructure may change as a result of temperature.

Conducting experiments with the intent of determining the stress-strain response of viscoelastic cellular solids requires the ability to produce consistent strain-rates as well as stable temperature environments. For quasi-static rates ($\dot{\epsilon} < 10^0$ s^{-1}), experiments are performed with a

screw or hydraulically driven load frame. Thermal chambers can be used in tandem with load frames to provide constant quasi-static rates across a temperature range. The load frame can be displacement controlled, so densification of the sample is assured. Additionally, an unloading hysteresis plot can be accurately measured. Intermediate rate results (10^1 s^{-1} > $\dot{\epsilon}$ > 10^2 s^{-1}) are achievable with drop-towers. This method relies on the potential energy of a falling anvil to load a sample, and the height of the anvil can be adjusted to account for larger impact velocities and higher strain-rates. It is worth noting that depending on sample thickness in the loading direction, a constant strain-rate may be unachievable. Therefore, instantaneous strain-rate through the elastic region is typically used to determine the strain-rate applied to the sample and ensure the proper loading rate was within the desired intermediate regime. To account for a temperature variable, drop tower experiments may be performed in a thermal chamber, or samples may be stored in a thermal chamber for later testing. For the latter technique, it is important to understand the role heat dissipation will play as samples are transferred from the thermal chamber to the experimental setup. Since polymers have low impedance and cellular polymers are filled with a fluid, heat dissipation or concentration occurs quickly. Dynamic results ($\dot{\epsilon}$ > 10^3 s^{-1}) are performed with Kolsky (or Split-Hopkinson pressure) bars that are often modified to produce results with softer materials [12, 15]. Performing dynamic experiments on viscoelastic materials

frequently results in a larger critical stress value than experiments performed at slower rates [12]. The role of temperature is observed to effect these responses independent of experimental rate, producing a stiffer, more brittle system at low temperatures, and a softer, more compliant system at higher temperatures [3, 10, 16]. This is a result of a polymer's glass transition temperature, which changes the material's stiffness. At colder temperatures, polymers display a larger stiffness modulus, whereas at hot temperatures, polymers are more rubbery and soft. These results are often verifiable with dynamic mechanical analysis machines (DMA). Beyond temperature, material cellular structure characteristics also play a role in the stress-strain response. Microstructure features including density, pore size, and cell-wall aperture yield changes to the length of the plateau region, location of the densification region in the stress-strain curve, and the overall critical stress value and elastic modulus [3, 11]. This work looks to develop a relationship between a cellular solid's microstructure and its temperature with respect to its protective capabilities, while maintaining a constant, intermediate strain-rate.

The design of the porous matrix within cellular materials also plays a role in the loading response [17]. For foams, two main matrix/cell types exist: open cell and closed cell. Open cell matrices involve interconnected webs of cell walls and void spaces, where pores are joined together. This allows the fluid inside the structure to move easily between pores and flow in and out of the matrix, only hindered by the aperture size of the pores. Closed cell foams consist of matrices filled with individual pores that are separated from the neighboring pores through cell walls. While open cell foams allow interior fluid to be released when the strain-rate is slow enough to maintain laminar flow, fluid within closed cell foams is trapped within each cell and is pressurized as the matrix/pore is compressed [17]. This can drastically affect the compressive strength of each individual foam type. These matrix changes and cell types can lead to various classifications for each composition. For example, closed cell foam matrices may break rather than flex, as the trapped air inside forces its way out of the cell structure, resulting in a longer plateau due to the escaping fluid released from the broken pores [17]. One important concept to remember while analyzing cellular materials is the role fluid dynamics plays in the loading response. Depending on cell wall aperture, interior fluid (open cell) or trapped fluid (closed cell), may be unable to escape at a rate above the experimental design. Previous analysis on the materials used for this study indicate that the loading rate required to produce a change in fluid flow rate (subsonic to supersonic) is outside of the loading rate bounds used here. Foams where fluid flow rate is a factor can see increased stress within the cellular structure [18]. Several other works have documented the role various laminar fluids play in the reaction of cellular solids under strain-rates, including changes in fluid type (non-Newtonian vs. compressible) and changes in molecular chemistry [19–22].

In this work, the intermediate stress-strain response of two open-cell polyurethane foams is analyzed over a range of temperatures. These foams are manufactured and provided by Team Wendy®, designers and suppliers of combat helmets currently used throughout the United States military. A new composition, named 98A, is directly analyzed alongside the current foam liner material, ZAP. The stress-strain response of these two foams are examined across six temperatures in an effort to characterize the differences in the material's protective properties. The temperature range chosen for these experiments reflects the various application spaces where these helmets are deployed. Experiments were conducted using a custom built drop-tower assembly and accompanied with accelerometers, high speed cameras, and a thermal chamber. Additionally, X-ray computed tomography (XCT) was performed on both post-mortem and pristine samples to explore qualitative microstructure changes to characterize foam's temperature dependent properties and failure mechanisms.

Experimental Methods

Material Properties

The materials in this study are open-cell polyurethane helmet liner foams, with individual properties displayed in Table 1. Additionally, a soft, flexible foam is included in the helmet construction, however, this foam is used primarily to provide comfort to the wearer, and is not analyzed in this study. The comfort foam and the selected protective foam (98A or ZAP) form a conglomerate laminate, with the outer edge of the protective layer interfacing with the rigid shell of the helmet. Current helmet models use ZAP, and 98A is being investigated as a potential next-generation material. Specimens used in this study were rectangular prisms, measuring approximately 30 mm×30 mm×12.7 mm.

Table 1 Material Properties

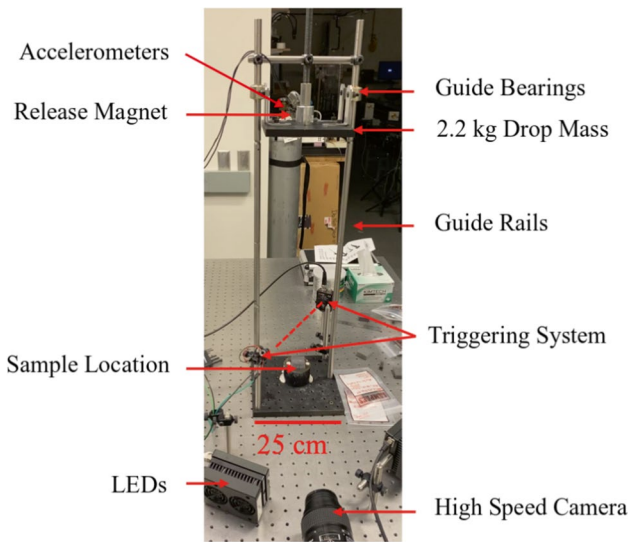| Material Property	ZAP	98A
Density (kg/m^3)	48	224
Average Pore Diameter (μm)	508 ± 153	68.8 ± 22.7
Volumetric Density (% air)	96	88

**Fig. 2** The experimental setup used for intermediate loading

Drop Tower Design

For these experiments, a custom drop tower was built using optical rails, an aligning breadboard, falling mass and guide bearings. The falling drop mass was secured in place via an electromagnet. The height of the 2.2 kg falling mass was set at 0.35 m to produce a consistent impact energy of 7.5 J at 2.6 *m/s* and an average strain-rate of 200 s^{-1}. These values were selected to mimic potential loading conditions that

would occur during the lifespan of the helmet liner pad. A Shimadzu TCE-300 thermal chamber was used to condition the foam samples at the selected experimental temperature. Prior to each experiment, the thermal chamber was set to the predetermined temperature and given time to equilibrate. During experiments, samples were placed in the chamber for one hour to reach steady-state. Individual samples were then removed from the chamber and drop tower tested within 30 seconds. A diagram of this design is shown in Fig. 2.

Due to the inherently low thermal impedance of porous, cellular structures, a basic heat transfer protocol was leveraged. The primary goal was to ensure that samples, once extracted from the thermal chamber, maintained the desired temperature during subsequent dynamic loading. Simplified heat transfer equations and experimental thermocouple readings were used to confirm that the sample temperature stayed within a five-degree Celsius range of the initial steady-state value during drop-tower investigations. As depicted in Fig. 3, results show that samples tested within 30 seconds of exiting the thermal chamber consistently fell within the specified temperature range. To accommodate testing at -20 °C, the thermal chamber temperature was adjusted to -27 °C. All samples underwent loading within the first 30 seconds post-removal, with each sample undergoing extraction only once. Importantly, no samples were subjected to thermal cycling.

Force data was collected using accelerometers. Two accelerometers (a tri-axial 10 mV/g 200 g saturation and a 1 mV/g uni-axial 5000 g saturation) were also used and attached to the drop mass. The acclerometers were attached to the top

Fig. 3 The heat transfer curves for each sample composition
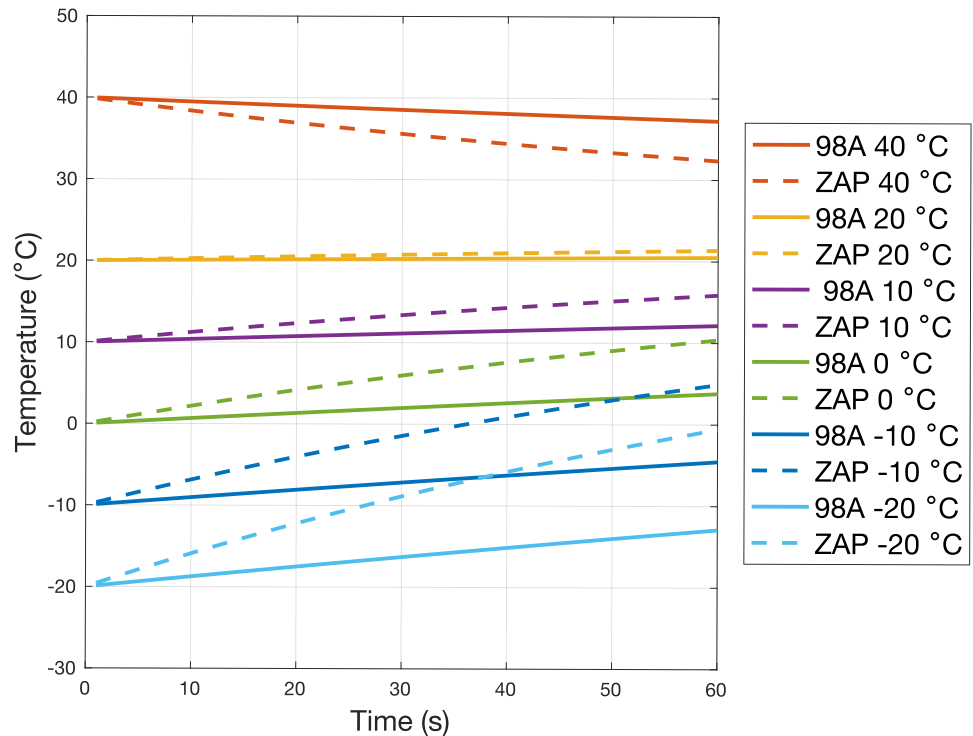
surface of the falling mass via Loctite super glue, and were inspected regularly to ensure their connection to the plate was fixed. Data was read from the accelerometers using a Lecroy HDO 4034A oscilloscope, with a sample time of two seconds and a sampling rate of 500 kHz.

Specimen Details

The prepared specimens for these experiments were produced by Team Wendy® and cut using a die-press. Samples were cut into 30x30x12.7 mm³ prisms. To aid with the high speed imaging, the sample surface facing the camera was lightly sprayed with thin layer of white water-based acrylic air-brush paint. This provided contrast for Digital Image Correlation (DIC), as the porous surface provided natural speckles and feature creation. In the case of the higher-density 98A composition, the white paint was used to create the speckles, since the pores on the 98A composition were too small to be used as DIC features but the provided sample material was black, thus providing contrast. An image of the painted specimen is shown below in Fig. 4.
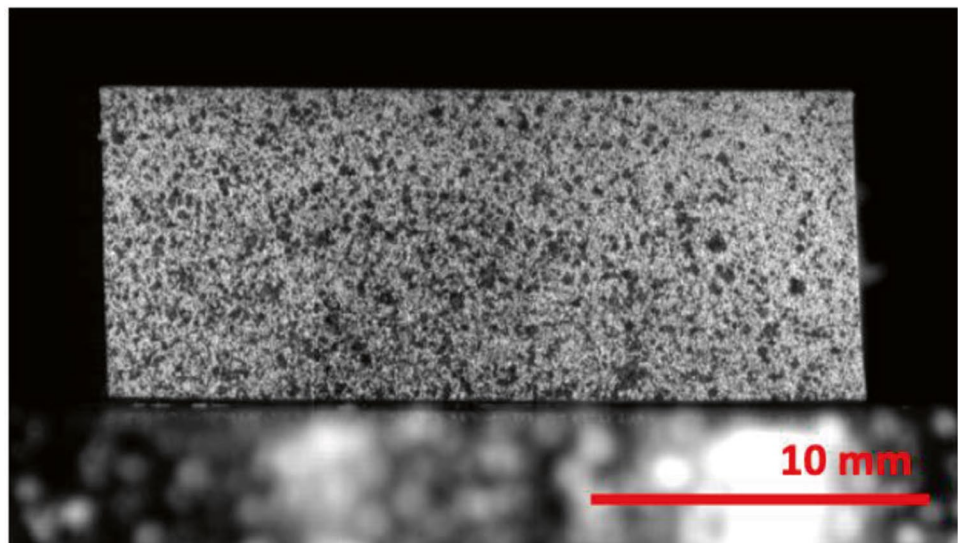
Full-Filed Imaging

All experiments were imaged with a Photron Fastcam SA5 with a frame rate of 10,000 fps and 150 mm lens to extract *in-situ* full-field displacement data through DIC. The system

**Fig. 4** Properly painted samples displaying adequate surface contrast for the DIC software
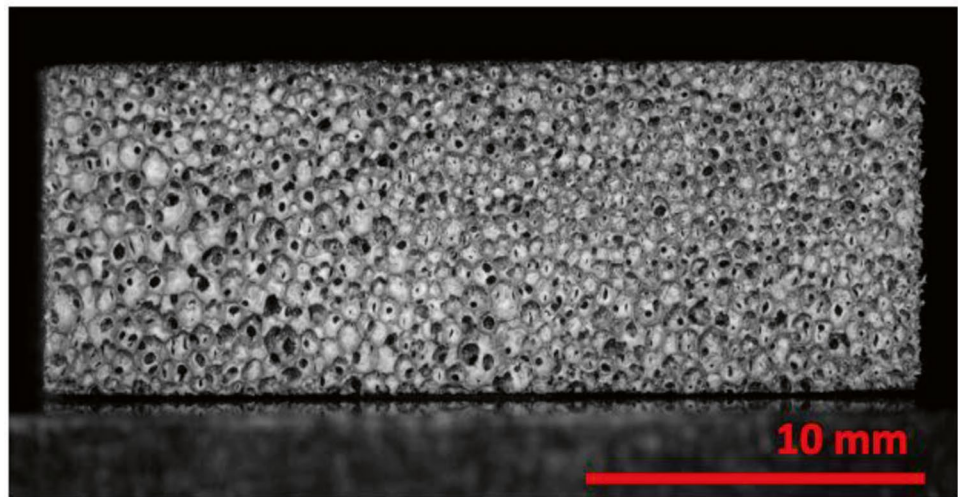
ZAP

98A

was triggered using a electrical circuit connected to the tower's electromagnet. DIC uses the gradient in grey scale values across a region of interest to create a unique set of features which are then tracked for use as displacement data. This data can be manipulated to a number of different experimental parameters [23]. In order to track these displacements during the experiment, a control (or reference) state is calculated before any loading or movement has begun. Since the visible pores of the samples have a difference in grey scale, the pores themselves are able to be used as the features for the specimens. The frame rate used for all experiments, determined by the loading rate, was 10,000 fps. The camera was positioned perpendicular to the loading plane with the sample covering 75% of the field of view. The specific distance from the loading plane to the sensor of the camera was determined using the thin lens approximation based on the 105 mm focal length lens and the ratio of the size of the sensor with respect to the sample size.

In order to verify the experimental DIC setup, two cameras were placed on opposite sides of the specimen during a drop test. Analyzing the opposite sides of the specimen along the same plane should result in the same values for longitudinal and lateral displacement if there was no out of plane displacement (i.e. bowing of the sample, or uneven loading conditions), and this was verified. An image of this experimental setup is shown below in Fig. 5, and the results
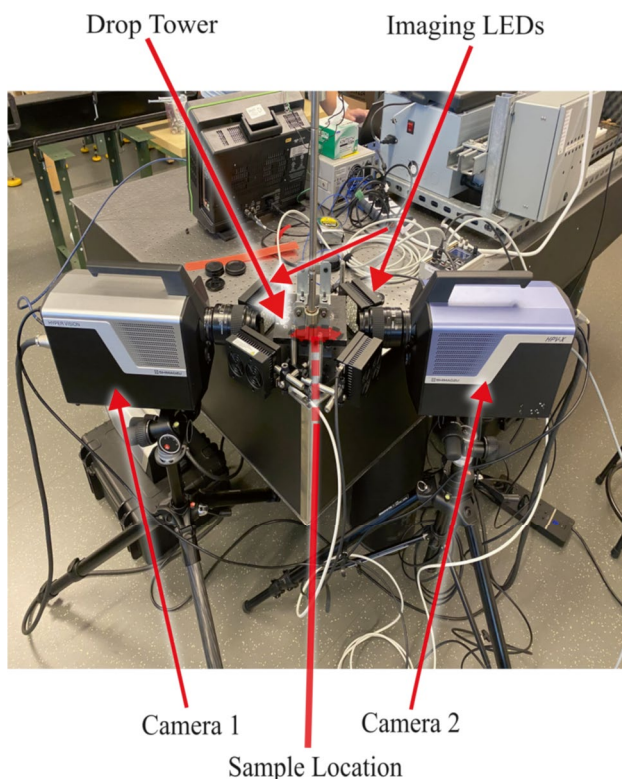
Fig. 5 DIC setup showcasing the dual camera approach to out-of-plane displacement accountability

of the experiment in Fig. 6. The results show there was negligible out-of-plane deformation for these experiments.

Due to the large strain in these experiments, incremental DIC was required. If the reference image was not updated as the specimen was loaded, the change in control volume and loss of speckles/features from one frame to the next was too great for the software to track the original features. Updating the reference frame allowed for the correlation to complete throughout the entire experiment; however, by using the foam's pores as features, the pores both change shape and disappear as compression continued to the densification regime. When this occurred, the loss of features was great enough that the full-field strain data was unusable past 30 percent compressive strain. To account for this, digital extensometers were used to measure the global strain values for longitudinal strain and are shown in Fig. 7. The DIC settings used for each sample type (ZAP and 98A) are listed below in Table 2.

The digital extensometers supplied global strain and displacement. The strain calculated from the digital extensometers was corroborated with manually-computed average full-field displacement data below 30%. The comparison revealed a difference of less than 5%. While full-field strain data became unreliable beyond 30% compressive strain, the full-field displacement data remains potentially valuable for future analyses.

Microtomography

X-ray Computed Microtomography (XCT) is a non-destructive technique used to characterize microstructure properties of various materials [24]. While XCT is often used for materials with a high impedance, it can be adapted to accurately characterize soft polymer systems and provide insight into their cellular structure. For this work, a Zeiss XRadia 520 XCT machine was used to analyze samples. Since the impedance of polymer foams is very low, extra care was taken during setup. This involved analyzing the histogram to ensure proper grey values to ensure contrast between cell walls and pores, and making the distance between the machine source and sample as small as possible to provide the resolutions below 3 μm. Additionally, recipe files were used so that scans could be repeatable. Since a resolution of 3 μm was desired for each scan, the scan time was selected to be 10-14 hours in length. Each sample analyzed had two different scans performed. The first was a warm up scan, designed to acclimate the sample to the machine's temperature, ensure the sample's orientation was correct, and prevent the sample from thermally expanding during the analysis scan, which followed the warm up scan. Due to the chemical differences between the two studied foam compositions, each sample type required some adjustments to the general setup. Table 3 details the different

Fig. 6 DIC out-of-plane results highlighting the same measured displacement from both sides of the impacted sample
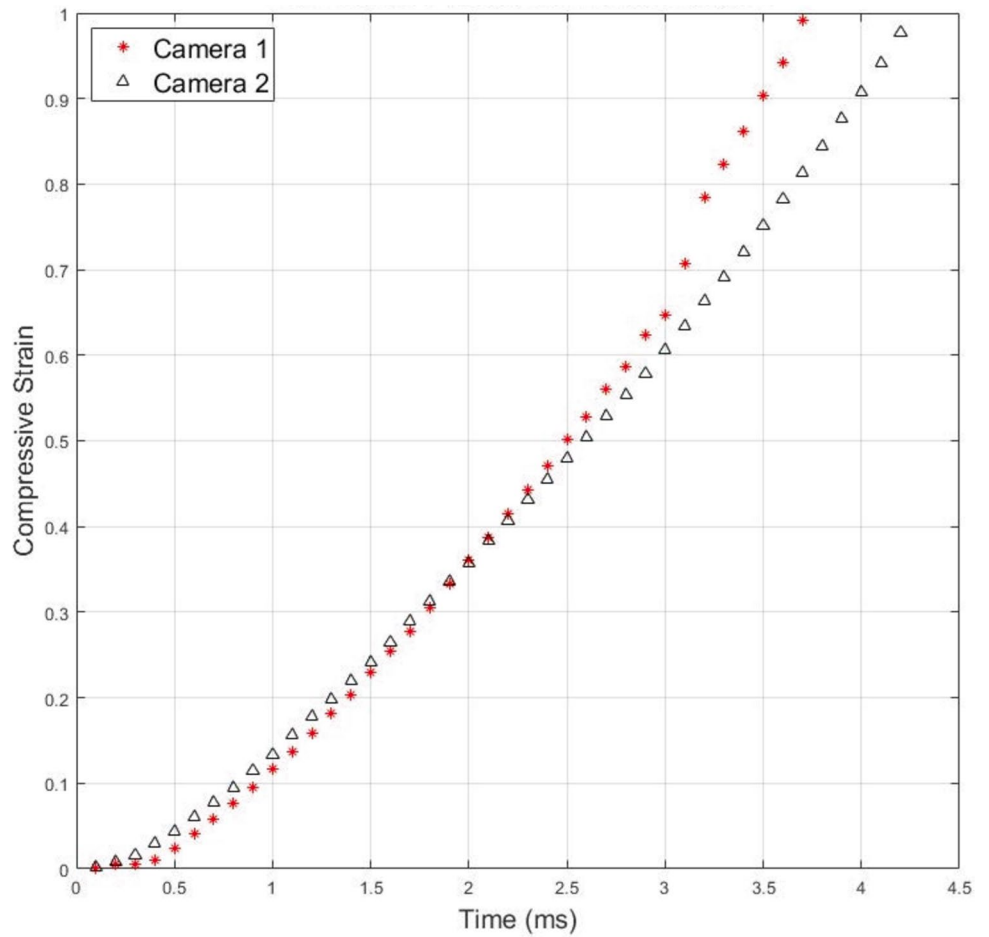
setup procedures followed and resolutions achieved for each sample type. Following the XCT imaging, analysis was done using Dragonfly ORS, a 3D reconstruction software. A series of filters were applied to each image stack so that regions of interests could be established between the cellular walls of the examined specimen and the porous, open spaces. The low impedance of the foam made identifying regions of interest difficult, and therefore several filters had to be used.

Fig. 7 DIC ROI used to establish global strain values at large deformation
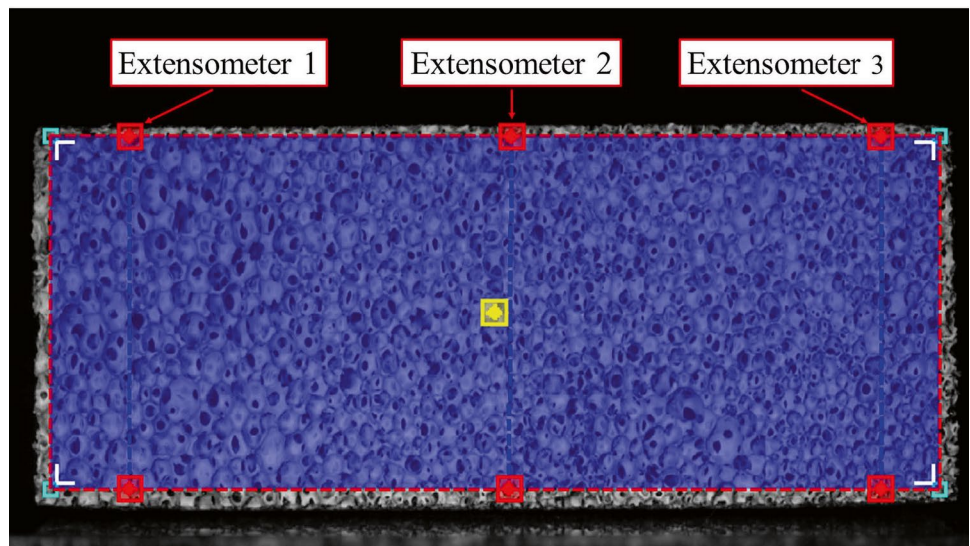
Table 2 DIC Parameters

DIC Parameter	ZAP	98A
Pre-filtering	Gaussian	Gaussian
Subset size	21	31
Step size	10	10
Correlation criteria	ZNSSD	ZNSSD
Shape function	Affine	Affine
Interpolation function	LBS[a]	LBS
Total images	400	400
Pixel to mm conversion	23	23

[a]Local Bicubic Spline

Results and Discussion

The acceleration curves from the drop tower experiments are shown in Figs. 8 and 9. The acceleration response of both foams changes drastically with respect to temperature. For the higher density foam (98A), the samples loaded at 0, 10, and 20 °C saw the lowest values of peak acceleration, whereas samples tested at max cold and max hot temperatures saw the highest values. This reflects the temperature dependent characteristics of the material structure. In colder temperatures, the foam becomes stiffer, resulting in a reduced strain response to increased loading. Conversely, in hotter environments, the structure becomes less rigid, leading to a higher strain response under load. In both temperature extremes, the material response produces peak acceleration values exceeding 100 g's.

Accelerometer Analysis

When analyzing the acceleration profile for the ZAP composition, a much steeper parabolic curve is seen in densification portion for all temperatures when compared to the response of the 98A. The increase in peak acceleration between the 20 and 40 °C samples indicate that for the 40 °C sample the foam's cellular truss

Table 3 XCT Paramters

XCT Parameter	ZAP	98A
Sample Size (mm^3)	1230	602
Resolution (μm)	1.99	1.03
Scan Length (hrs)	12	10
Post Processing Filters	ZAP[a]	98A[b]

[a]Histogram Equilization (used to normalize grey values), Median Shift (used to highlight contrast), Membrane Projection (used to highlight porous boundaries)
[b]Median Shift, Membrane Projection

structure was unable to provide an adequate cushioning response and instead was crushed quickly, resulting in more of the drop mass's kinetic energy being transferred to the anvil instead of the foam sample.

Stress-Strain Analysis

After analyzing the acceleration profiles, a stress-strain curve was created. This was done by combining the results taken from DIC displacement data and the accelerometer results. The displacement was converted to strain, and the stress was calculated through the following equation:

$$\sigma_{axial} = \frac{F}{A_{sample}} \tag{1}$$

where:

$$F = a_{accel} \cdot M_{plate}. \tag{2}$$

These results are displayed in Fig. 10. A zoomed-in view of the elastic and plateau regions are provided for clearer visualization.

At -20 °C, the 98A composition displays a linear stress-strain response and does not generate a densification region. The linear response to the specific combination of temperature and loading rate indicates a purely elastic response as the samples appeared to fully recover their initial shape and height. Subsequent XCT analysis suggested this as well, revealing no internal damage and emphasizing the recoverable deformation.

This is also traceable to the acceleration curves, where the overall acceleration can be viewed as a triangle consisting of an approximate linearly increasing initial slope, and then a decreasing linear portion with a steeper slope. The shape here highlights an absence of a plateau region, suggesting that the foam displays only an elastic loading and unloading. Remaining in the cold temperature range, (-20 to 0 °C) the foam displays an elastic modulus that is steeper than the warmer samples. This result is also visible in the acceleration curves, where the initial acceleration of the plate after impact (time < 1 ms) is slightly higher than the warmer temperatures. Furthermore, the experiments performed at colder temps result in less compressive strain, once again showing a relationship between the foams mechanical response and the temperature of its environment. A shift from an elastically-dominated response profile to a more viscous one develops as the temperature increases. The regions of the stress-strain curve (linear elasticity, plateau, densification) become more defined as temperature changes from 10 to 40 °C. Additionally, the critical stress value drops steadily implying that the initial elastic response and peak acceleration associated with the impacting plate has decreased as well. The peak compressive strain increases as temperature increases, which is seen in the acceleration

**Fig. 8** Acceleration profile for 98A taken from accelerometers
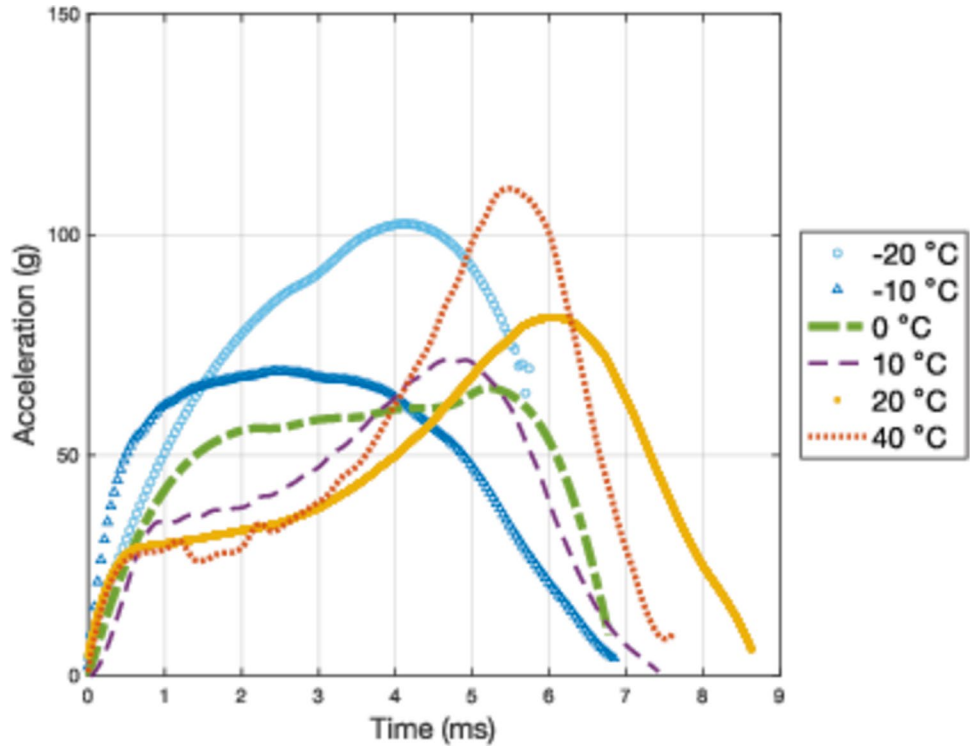
curve as the time needed to generate the peak acceleration. It is important to note that these results do not suggest that the 98A composition would not generate a densification profile at colder temperatures. The densification regime would be created if the either the dropping weight or the height of the drop tower was increased.

When analyzing the ZAP composition, all samples reach densification. It is easy to see the connections between the acceleration profile and stress-strain profile here, and the relationship each curve has with temperature. Since each temperature range produces a full viscoelastic material stress-strain curve, several conclusions can be drawn about

Fig. 9 Acceleration profile for ZAP taken from accelerometers
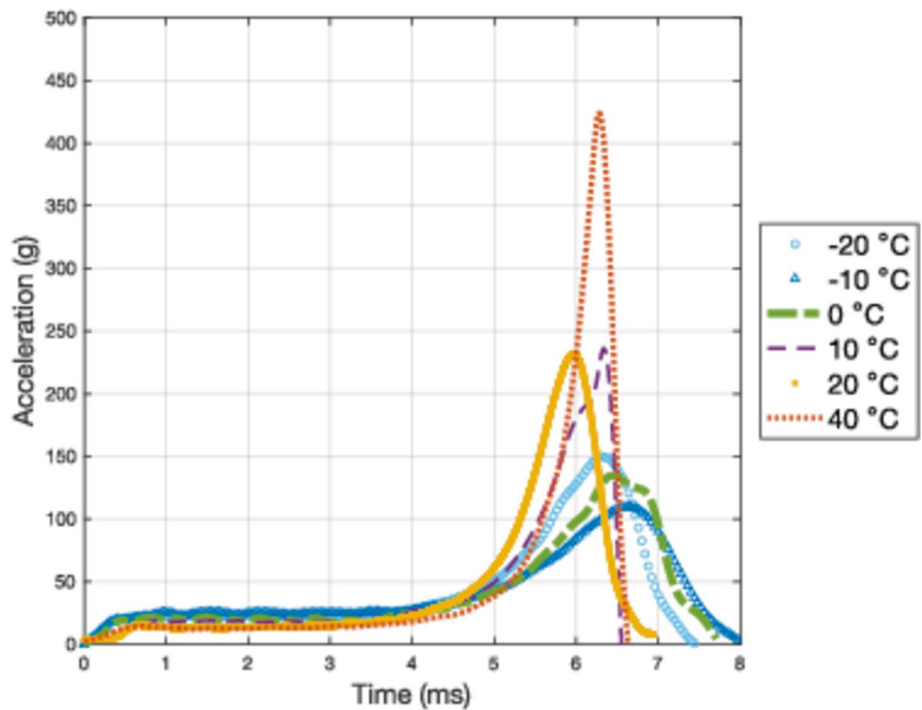
Fig. 10 Stress-strain profiles: (**a**) ZAP composition stress-strain profiles for the entire experiment. It is suspected that the 40 °C sample was too soft to absorb significant energy. (**b**) ZAP composition stress-strain profile zoomed in the elastic and plateau regions of the experiment. (**c**) 98A composition stress-strain profiles. (**d**) 98A composition stress-strain profiles zoomed in the same strain region as ZAP composition for comparison
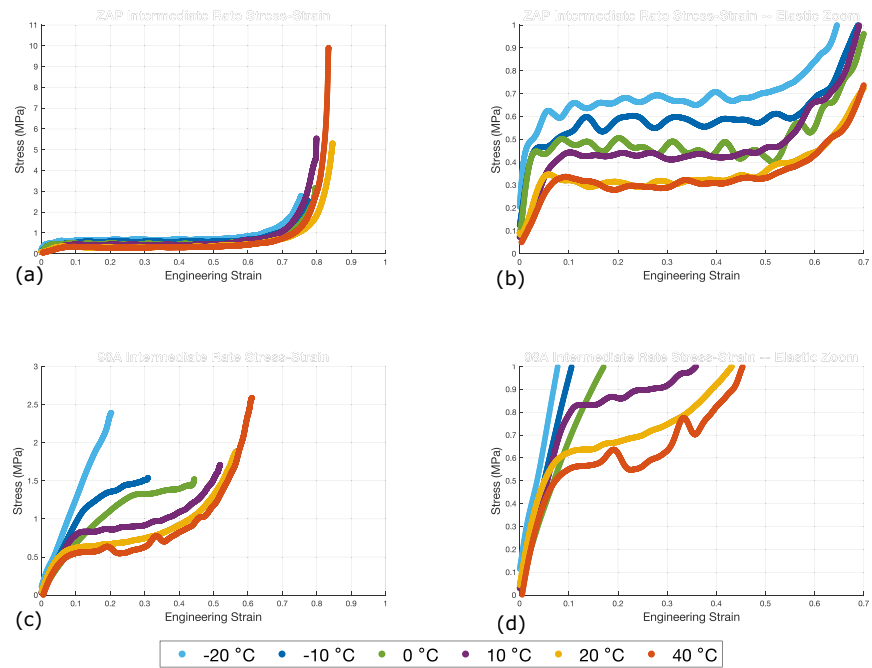
this composition. Initially, a validation is seen with the results at the 40 °C sample, which displays both the highest peak acceleration and stress value. This again reflects the notion that energy was instead transferred through the foam into the anvil, implying that the material provided little energy absorption. Unlike the 98A composition, the less-dense ZAP does not exhibit a pure elastic response at any of the temperature range, likely due to the difference in density. However, similarities can still be drawn between the two compositions, as the ZAP samples display the same trend of decreasing elastic moduli stiffness and decreasing critical stress as temperature increases. Additionally, the onset of densification occurs at increasing strain values as temperature increases suggesting that this composition also becomes softer and the response becomes more viscous-dominated.

The distinctive characteristics of these foams are evident in the high speed images captured during deformation, as illustrated in Fig. 11. The response of the two foams differ noticeably. The images were taken during a 20 °C experiment, and the colored dots below each image, next to the time stamp, are plotted on the corresponding stress-strain curve. The transition between 25 and 65 milliseconds is particularly prominent in the ZAP composition, highlighting the extended plateau region discussed earlier. In contrast, the 98A composition exhibits a reduced plateau region, undergoing densification before the ZAP composition completes its plateau phase.

It is important to note that the glass transition temperature for polyurethane based poly-chains occurs around 0 °C [25]. While the overall chemical composition of each sample type is unknown (and proprietary), the base material's T_g imply that both compositions have a T_g within the

range of temperatures studied here. A further analysis on the role the T_g plays in these materials would be useful for further modeling efforts, but is outside the scope of the work presented in this paper.

Energy Absorption

The energy absorption properties of each composition were also calculated by integrating the stress-strain curve of each experiment. The strain-energy density, $\hat{u}$, is determined by:

$$\hat{u} = \int_0^{\epsilon_f} \sigma(\epsilon)d(\epsilon). \tag{3}$$

The integration of the stress-strain curve to obtain the strain energy density used the trapezoidal method, and was performed for both the entire stress-strain curve and also done with the curves to 65% compressive strain. The results for both compositions are shown in Fig. 12. By employing a stress-strain curve integration approach, the earlier conclusions regarding the lack of energy absorption or work performed by the foam during the 40 °C experiment can be substantiated. This is evident as the calculated strain energy density does not exceed twice the value observed in the 20 °C experiment, contrary to what was implied by the acceleration curves. This suggests that minimal energy absorption occurs during the densification process. To ensure a consistent comparison across all curves before the onset of densification, a specific point along the strain axis was chosen. Given that the densification regime is marked by the shift from a constant stress value to an exponentially increasing one, a 65%
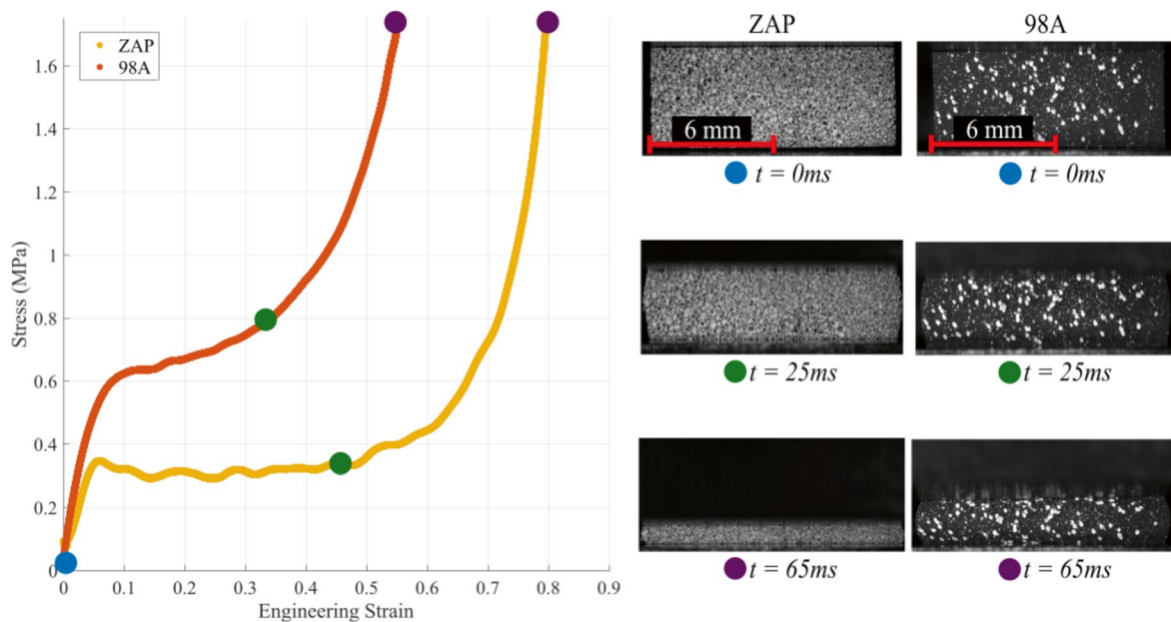
Fig. 11 Images of 20 °C ZAP and 98A samples at various compression states, shown next to their stress-strain response, respectively

compressive strain was selected. The selection of a 65% strain as the cutoff for energy absorption calculations in the ZAP composition was informed by an analysis of the densification region onset. Specifically, a central difference method was employed to identify the onset of the densification region, which is marked by a significant change in the stress-strain curve's slope. The analysis revealed that for all ZAP composition experiments, the initiation of a notable slope change – exceeding 2.5 MPa/strain – consistently occurred within a proximity of 1% to the 65% strain mark. This consistency across experiments underpinned our decision to adopt 65% as the strategic cutoff point. This approach ensures that the entirety of the densification region, which poses challenges in terms of quantification and inclusion due to its variability, is methodically removed. As a result, the determination of 65% as the cutoff enables a standardized comparison of trends across samples, by anchoring the analysis at the end of the plateau region. Moreover, this comparison point underscores the influence of temperature on energy absorption by highlighting its connection to a steep elastic modulus and the critical stress value. Post-densification, the force from the drop mass and resultant stress no longer contributed to strain energy, rendering data points beyond this region attributable to energy transfer rather than absorption.

For ZAP, samples that had the most area under the stress-strain curve were those analyzed at cold temperatures. The decreasing change in the energy absorption profile also highlights the overall stiffness change of the composition. The analysis for 98A displays a different relationship between temperature and strain energy absorption. It is evident that a sample with the largest critical stress that also reaches

densification through loading would produce the largest energy absorption value. This is seen in the logarithmic shape of the graph, which shows an increasing value as temperature increase but then appears to peak at 20 °C, indicating that this is the optimal temperature range for the material performance capabilities. Since none of the samples reached 65% densification, the comparison point here was unnecessary. This point would have provided good comparison should the response for each sample reached densification. Although the strain energy density parameter is a good metric for comparing the energy absorption properties of protective materials, it does not provide an in-depth analysis of the microstructure changes that may occur during the loading process.

Microstructure Analysis

The microstructure analysis performed with XCT yielded several key findings. As shown in the pristine 2D sample images, Fig. 13, each composition had a distinct cell structure and pore size. Due to the nature of the experiment (non-repetitive drop test), the microstructure of each sample maintained much of its original design and structure. However, under cold temperatures (-20 °C), ZAP composition samples showed cell wall damage including bent/buckled and broken cell walls. The broken cell walls had sheared away from their connections, resulting in webbing that no longer provided structural support. It was estimated that roughly 15% of the cell walls (viewed as simple truss networks) obtained irreversible damage in the form of broken connections. The mechanism behind this damage is expected to be either fracture or buckling shear failure, however without *in-situ* XCT
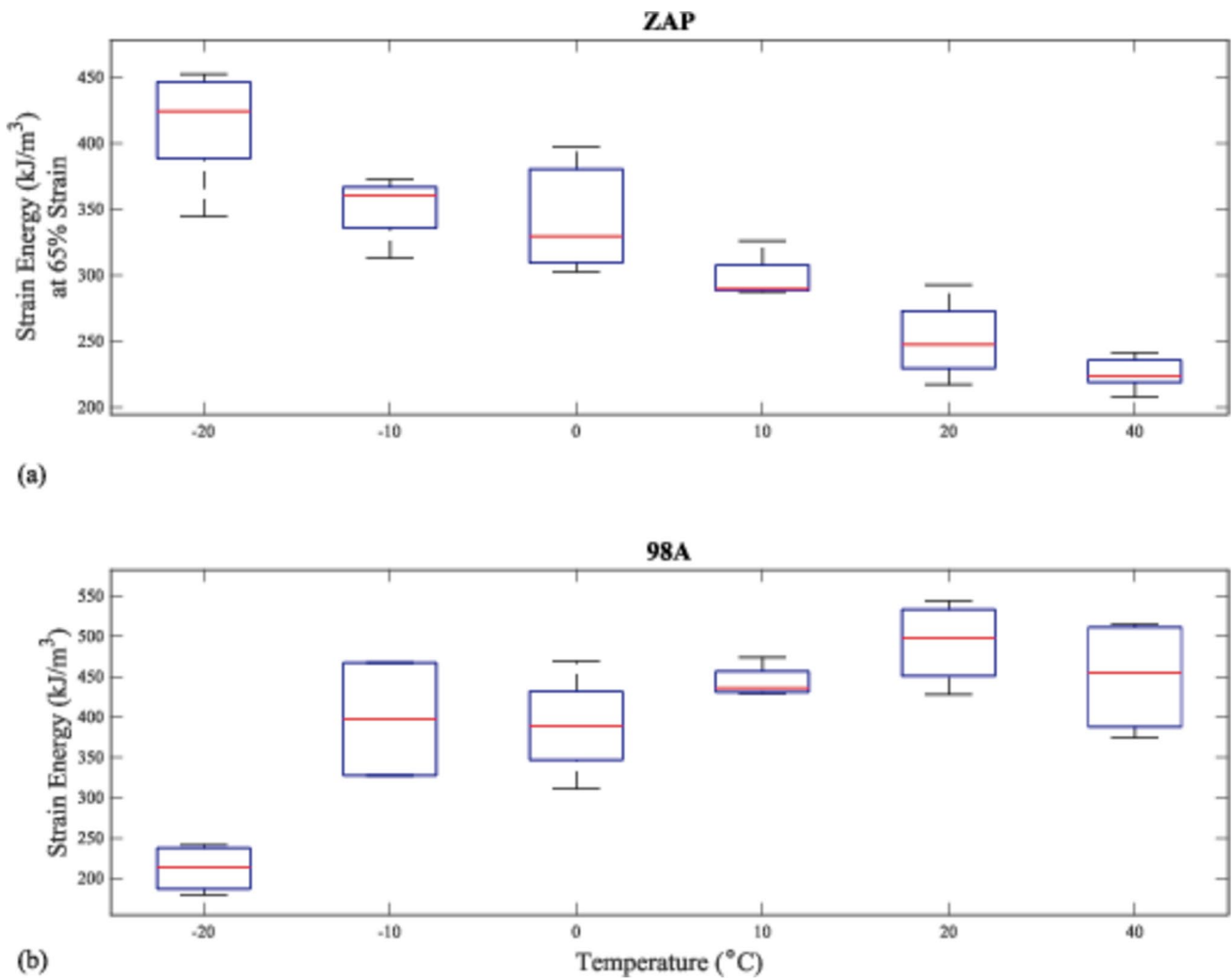
Fig. 12 Energy absorption: (**a**) Energy absorption of ZAP to 65% compressive strain to highlight the comparison in plateau length and critical stress value. (**b**) Energy absorption across the entire stress-strain curve for each temperature. Note the 98A composition never reached 65% compressive strain

analysis, this is not verifiable. A direct comparison of ZAP cold samples to ZAP hot samples revealed that ZAP hot samples contained no shear failure, with only minor cell wall buckling. This finding supports previous conclusions that the stiffness of the foam was related to temperature. Additionally, these results also reveal that in cold environments, the polyurethane structure may become too brittle to support intermediate-rate compressive loads and will therefore break, thus presenting ideas that the main damage mechanism is fracture. This can also be a point of interest with respect to the strain energy profile, where energy from the drop mass is used to damage the cell walls of the foam, resulting in higher energy absorption values for the colder samples that experienced damage. Broken cell walls were not present in the hot samples because the material structure was more compliant and therefore deformed without much

resistance. The images presented in Fig. 14 display a 2D broken cell wall and several instances of broken cell walls in the 3D view, respectively.

The 98A microstructure investigations did not yield as significant of findings between pre- and post-drop scans. While instances of cell wall buckling were found, there were no cases of cell wall fracture or shear failure. This is likely due to the small deformation that occurred during the colder temperature experiments which kept the 98A sample in the elastic region of the stress-strain curve. Additionally, the absence of failure mechanisms could also be due to the high density of the composition, which allowed more cell walls to bear the loading force, preventing an individual wall from rupturing. It should be noted that 98A composition is likely not immune to damage, just that the loading rate was not sufficient enough or temperature low enough to instigate failures.
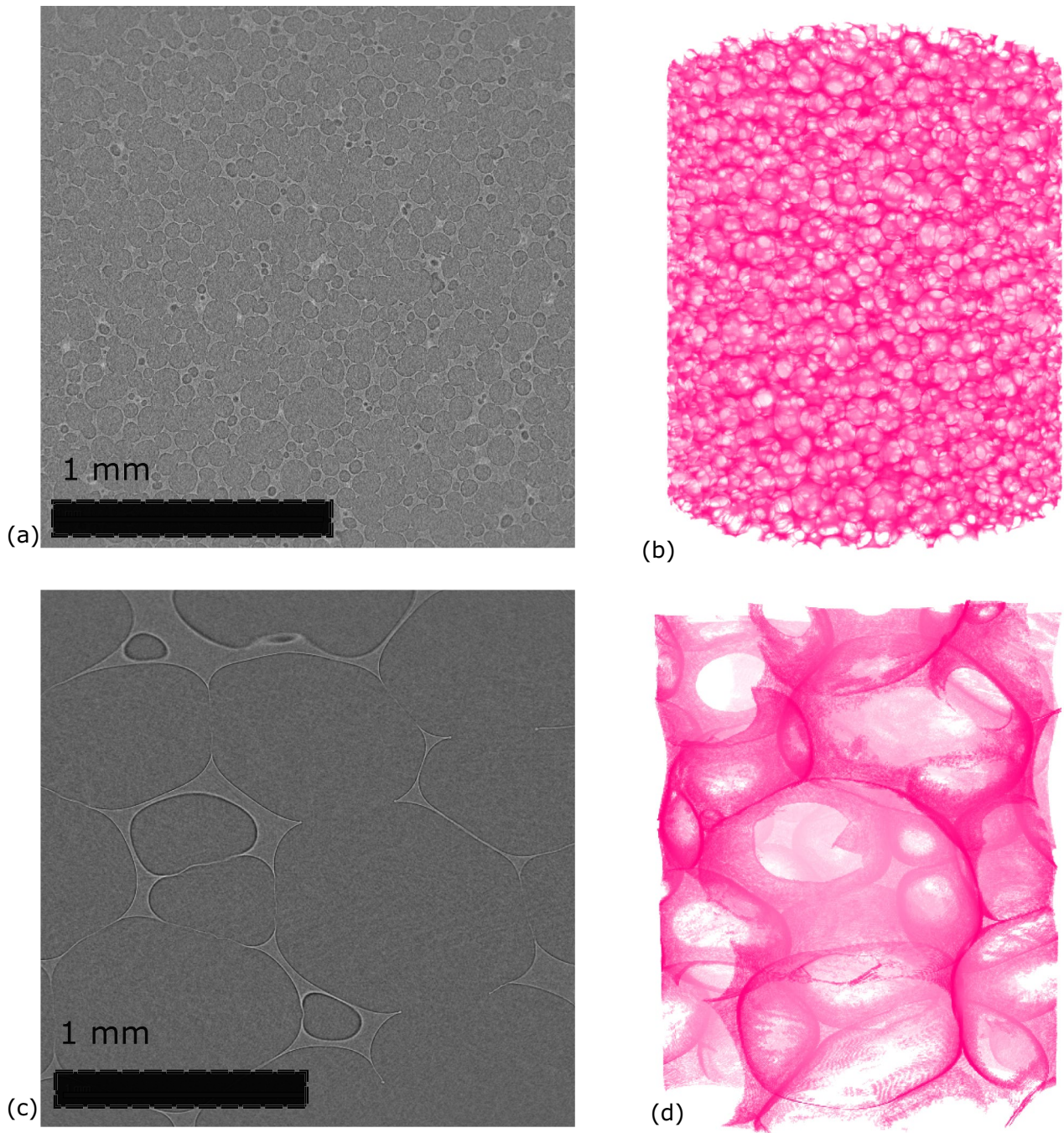
Fig. 13 Prestine samples from XCT: (**a**) 2D pre-filtered 98A composition, (**b**) 3D post-filtered 98A composition, (**c**) 2D pre-filtered ZAP composition, and (**d**) 3D post-filtered ZAP composition
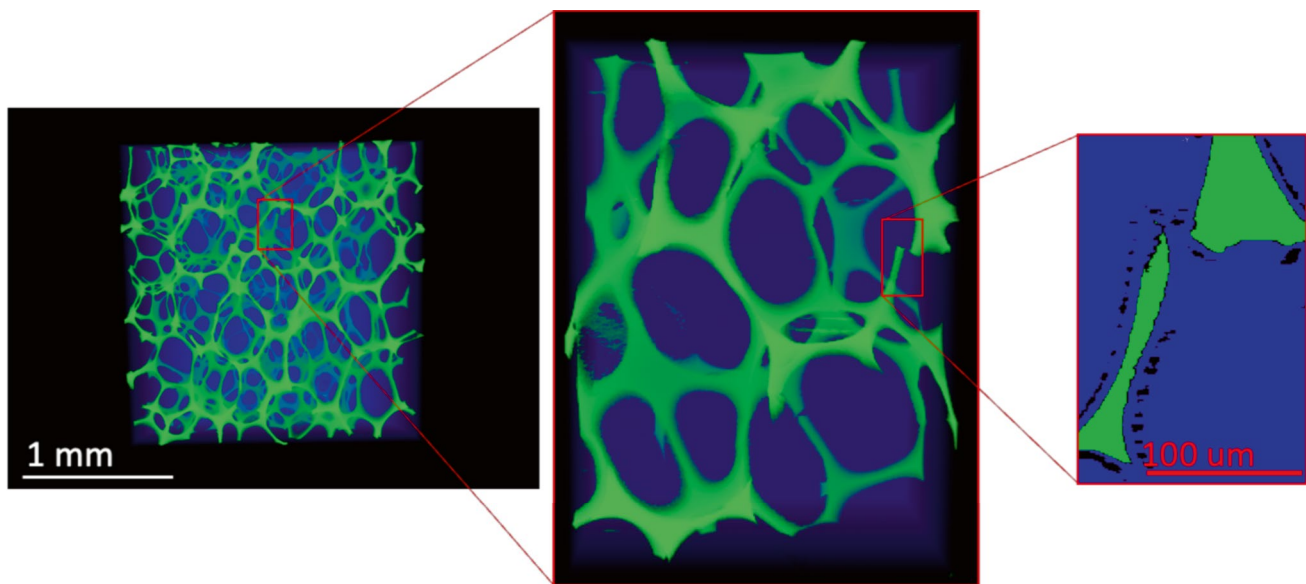
Fig. 14 ZAP composition post-mortem broken cell walls

Conclusions

The temperature dependent intermediate strain-rate compressive response of two polyurethane open cell foams was analyzed and quantified. A drop tower experimental apparatus was designed and implemented to produce the relevant experimental parameters, and multiple data acquisition techniques were used to derive various properties including microstructure changes, strain energy absorption, and stress-strain responses. High temperature was found to decrease the critical stress value and increase the global strain value, implying that temperature plays a vital role in the materials temperature dependent response by softening the cellular structure making it easier for deformation to occur. Moreover, colder temperatures were found to have an inverse effect, causing the samples to become brittle and stiff, resulting in low strain across 98A samples and shear failure in ZAP samples. These outcomes help create a correlation between the materials density and its dynamic loading response, suggesting that, when used as a protective material, polyurethane foam structures may be adverse to the wearer when under certain environmental conditions. Both foam compositions were compared directly and the results will be used in the future to improve the protective capabilities of military helmets. The use of XCT to analyze sample microstructure properties and changes was determined to be very valuable, as important failure mechanisms were found to vary across the experimental temperature range. Additionally, the use of XCT imagery presented unique viewpoints into the cellular network of pores and cell walls, allowing for accurate depictions of each composition on a micrometer scale.

Declarations

References

1. Ashby MF, Medalist RM (1983) The mechanical properties of cellular solids. Springer
2. Koohbor B, Blourchian A, Uddin KZ, Youssef G (2021) Characterization of energy absorption and strain-rate sensitivity of a novel elastomeric polyurea foam. Adv Eng Mater 23(1):2000797

3. Ramirez BJ, Gupta V (2018) Evaluation of novel temperature-stable viscoelastic polyurea foams as helmet liner materials. Mater Design 137:298–304

4. Gioia G, Wang Y, Cuitiño AM (2001) The energetics of heterogeneous deformation in open-cell solid foams. Proc R Soc Lond Ser A Math Phys Eng Sci 457(2009):1079–1096

5. Rahman O, Uddin KZ, Muthulingam J, Youssef G, Shen C, Koohbor B (2022) Density-graded cellular solids: mechanics, fabrication, and applications. Adv Eng Mater 24(1):2100646

6. Koohbor B, Youssef G, Uddin KZ, Kokash Y (2022) Dynamic behavior and impact tolerance of elastomeric foams subjected to multiple impact conditions. J Dyn Behav Mater 8(3):359–370

7. Liu DS, Chang CY, Fan CM, Hsu SL (2003) Influence of environmental factors on energy absorption degradation of polystyrene foam in protective helmets. Eng Fail Anal 10(5):581–591

8. Luan S, Kraynik AM, Gaitanaros S (2022) Microscopic and macroscopic instabilities in elastomeric foams. Mech Mater 164:104124

9. Gibson LJ, Ashby MF (1997) Cellular solids: structure and properties. Press Syndicate of the University of Cambridge, Cambridge, UK

10. Ramirez BJ, Kingstedt OT, Crum R, Gamez C, Gupta V (2017) Tailoring the rate-sensitivity of low density polyurea foams through cell wall aperture size. J Appl Phys 121(22):225107

11. Rusch KC (1970) Energy-absorbing characteristics of foamed polymers. J Appl Polym Sci 14(6):1433–1447

12. Koumlis S, Lamberson L (2019) Strain-rate dependent compressive response of open cell polyurethane foam. Exp Mech 59(7):1087–1103

13. Li X, Tao J, Landauer AK, Franck C, Henann DL (2022) Large-deformation constitutive modeling of viscoelastic foams: Application to a closed-cell foam material. J Mech Phys Solids 161:104807

14. Lu FD, Hua GJ, Wang LS, Jiang HY, Gao D (2019) A phenomenological constitutive modelling of polyethylene foam under multiple impact conditions. Packag Technol Sci 32(7):367–379

15. Song B, Chen W (2005) Split Hopkinson pressure bar techniques for characterizing soft materials. Lat Am J Solids Struct 2(2):113–152

16. Liao Z, Yao X, Zhang L, Hossain M, Wang J, Zang S (2019) Temperature and strain-rate dependent large tensile deformation and tensile failure behavior of transparent polyurethane at intermediate strain-rates. Int J Impact Eng 129:152–167

17. Rusch KC (1970) Load-compression behavior of brittle foams. J Appl Polym Sci 14(5):1263–1276

18. Tang M, Huang G, Zhang H, Liu Y, Chang H, Song H et al (2017) Dependences of rheological and compression mechanical properties on cellular structures for impact-protective materials. ACS Omega 2(5):2214–2223

19. Kaewpradit P, Kongchoo A, Chonlathan P, Lehman N, Kalkornsurapranee E (2021) Impact responses of an open-cell natural rubber foam impregnated with shear thickening fluid. SPE Polym 2:217–223

20. Hilyard NC (1971) Observations on the impact behaviour of polyurethane foams: II, the efffect of fluid flow. J Cell Plast 7(2):84–90

21. Hilyard NC, Kanakkanatt SV (1970) Mechanical damping in liquid-filled foams. J Cell Plast 6(2):87–90

22. Dawson MA, Germaine JT, Gibson LJ (2007) Permeability of open-cell foams under compressive strain. Int J Solids Struct 44(16):5133–5145

23. Sutton M, Orteu J, Schreirer H (2009) Image correlation for shape, motion and deformation measurements. Springer, USA

24. Nguyen T, Ghazlan A, Kashani A, Bordas S, Ngo T (2018) 3D meso-scale modelling of foamed concrete based on X-ray Computed Tomography. Constr Build Mater 188:583–598

25. Landauer AK, Kafka OL, Moser NH, Forster AM (2022) A materials dataset for elastomeric foam impact mitigating materials. Materials Data Facility